MICROWAVE INSTABILITY MODELLING FOR SOLEIL II

V. Gubaidulin*, A. Gamelin
Synchrotron SOLEIL, Saint-Aubin, France

Abstract

There are two main sources of high-frequency longitudinal impedance: coherent synchrotron radiation (CSR) and high-frequency NEG-coated resistive wall impedance. They can drive microbunching instability, which is a potential risk to maintaining stable and low energy spread beam. To address this, these effects are now integrated into the particle tracking code `mbtrack2`. This paper examines their impact on beam stability in the SOLEIL II storage ring, considering the combined influence of intrabeam scattering, low-frequency longitudinal impedance, and a harmonic cavity.

INTRODUCTION

SOLEIL II [1, 2], a 2.75 GeV fourth-generation light source upgrade with a design horizontal emittance of $\varepsilon_x <$ 100 pm rad (< 60 pm rad with full betatron coupling) is presently in the construction phase. Two operation modes are planned: 416 bunches with 1.2 mA per bunch; 32 bunches with 6.25 mA per bunch. In our previous paper [3], we addressed microwave instability (MWI) arising from broadband longitudinal impedance up to 100 GHz in the presence of intrabeam scattering and harmonic cavity bunch lengthening. At least two potentially important contributions were not included, namely, coherent synchrotron radiation (CSR) [4–7] in dipole magnets and the high-frequency part (< 5 THz) of the impedance of NEG-coated vacuum chamber [8–10].

SIMULATION AND IMPLEMENTATION DETAILS

Impedance Model

Details of the broadband SOLEIL II impedance model (< 100 GHz) can be found in [11]. It consists of two components: resistive wall contribution (computed with `IW2D`) and geometric contribution (computed with `CST Studio`, `GdfidL` and `ECHO3D`). Table 1 shows the dipole magnet parameters relevant to CSR impedance and wakepotential computation. SOLEIL II design includes 178 reverse bends with

Table 1: SOLEIL II Dipole Magnet Parameters Relevant to CSR

Dipole type	**Number**	L_{dipole}	R_{bending}	h_{halfgap}
short dipole	40	0.44 m	10.74 m	8 mm
long dipole	64	0.88 m	12.80 m	8 mm
superbend	12	0.87 m	12.68 m	4 mm

a bending radius of > 40 m, length < 0.15 m and shielding half-gap of 6 mm. Due to the large bending radius and short length, reverse bends contribute only a negligible amount to CSR impedance and, thus, are ignored.

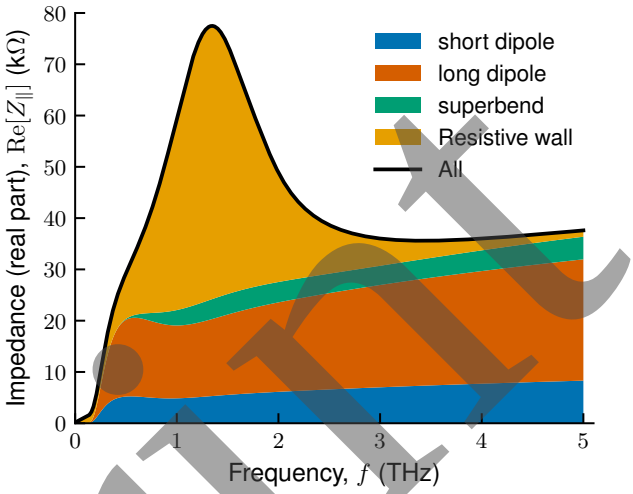

Figure 1: Total impedance (free space and shielding contribution from CSR and NEG-coated resistive wall (RW) impedance), real part (a), imaginary part (b).

Figure 1 displays the extension of the resistive wall component to higher frequencies (< 5 THz) and the contribution of CSR to the impedance (only the real part is shown in the plot). In SOLEIL II, we are expecting CuCrZr vacuum chamber ($\rho_{\text{CuCrZr}} = 2.08 \times 10^{-8}\,\Omega\,\text{m}$) with an effective radius [12] of $r_{\text{eff}} = 5.83$ mm for closed gaps of insertion devices. NEG-coating with 0.5 µm thickness and resistivity of $\rho_{\text{NEG}} = 1.25 \times 10^{-6}\,\Omega\,\text{m}$ is expected. Variation of thickness along the vacuum chamber does not change the impedance significantly for our value of resistivity, contrary to [9, 10], where the resistivity value is higher, and the THz peak is narrower and higher.

First estimation of CSR-driven MWI can be given analytically based on the dipole magnet parameters [7, 13], assuming

$$I_{\text{th}} = I_A \frac{\alpha_c \gamma \sigma_\delta^2 \sigma_s^{1/3}}{R_{\text{bending}}^{1/3}} \left(0.5 + 0.12 \sigma_s \sqrt{\frac{R_{\text{bending}}}{h_{\text{halfgap}}^3}} \right),$$

where $I_A \approx 17$ kA is the Alfven current, α_c is the momentum compaction, γ is the Lorentz gamma, σ_s is the rms bunch length, σ_δ is the rms energy spread.

With this formula for worst case dipole parameters of SOLEIL II, the threshold estimation is $I_{\text{th}} = 1.6$ mA for $\sigma_s = 15$ ps and $\sigma_\delta = 8.547 \times 10^{-4}$. For SOLEIL nominal parameters, we would obtain a larger value $I_{\text{th}} = 5.3$ mA mainly because the momentum compaction factor is four-five times smaller for SOLEIL II. This implies that CSR is more

* vadim.gubaidulin@synchrotron-soleil.fr

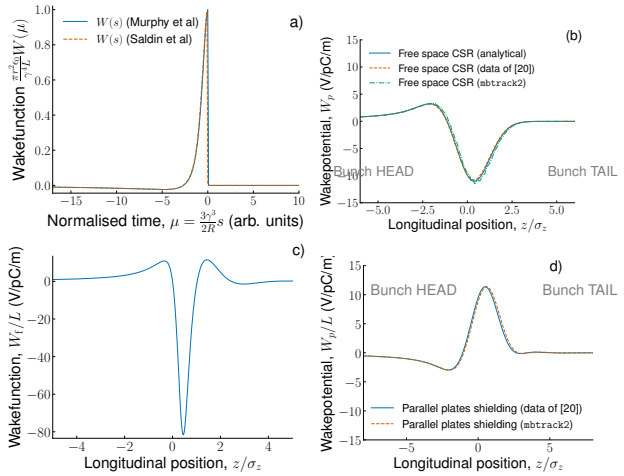

Figure 2: Benchmark of `mbtrack2` implementation of CSR wakepotential per unit length for parameters $R_{\text{bending}} = 5.36\,\text{m}$, $h_{\text{halfgap}} = 12.5\,\text{mm}$, $\sigma_z = 1.45\,\text{mm}\,(4.8\,\text{ps})$ [19]. a) Free space component of CSR wakefunction; b) free space component of CSR wakepotential; c) parallel plates shielding component of CSR wakefunction; d) parallel plates shielding component of CSR wakepotential.

important in SOLEIL II than in SOLEIL for operational parameters.

CSR Wakepotential Implementation

CSR contribution is usually divided into free space CSR and the effect of shielding. The free space CSR wakefunction has a very sharp peak around $t = 0$ [14, 15] with a magnitude $\propto \frac{\gamma^4}{\epsilon_0 \pi R_{bending}^2}$. After a characteristic time, the CSR wakefunction changes its sign and asymptotically decays to zero. This requires either a very fine sampling of bunch charge distribution and the wakefunction or a specific approach in calculating wake potential [16–21]. For our implementation in `mbtrack2`, we follow the wakefunction antiderivative-based approach outlined in [19, 20].

Figure 2 shows `mbtrack2` CSR wakepotentials, and their benchmarks with the results of [19]: free space CSR wakefunction (a), free space CSR wakepotential for a Gaussian bunch (b), parallel plates CSR wakefunction (c), parallel plates CSR wakepotential for a Gaussian bunch (d). Free space and parallel plates shielding components are shown separately. The total CSR wakepotential is always the sum of the two.

For this benchmark, a Gaussian bunch with rms bunch length $\sigma_z = 1.45\,\text{mm}$ was used with SOLEIL storage ring parameters assuming a bending radius of $R_{\text{bending}} = 5.36\,\text{m}$, and full gap of shielding plates $h_{\text{halfgap}} = 12.5\,\text{mm}$.

For free space CSR, the bunch will lose energy at the tail (negative wakepotential in `mbtrack2`) and gain energy in the bunch head. In addition to [19], we compare free space CSR wakepotential with an analytical formula given in [14]. The perfect agreement between our results, the data of [19], and the analytical formula in Fig. 2 validates the implementation of CSR wakepotential in `mbtrack2`.

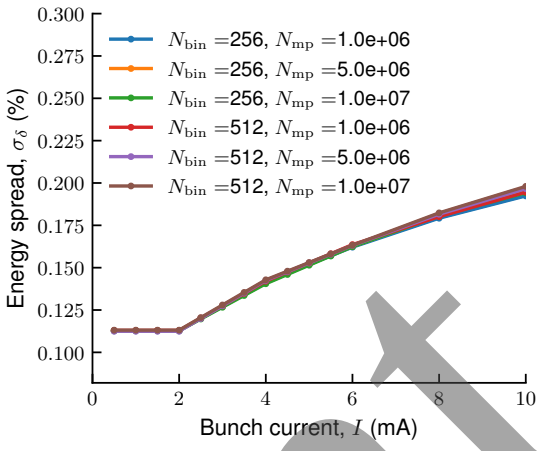

Figure 3: Convergence study for SOLEIL II CSR impedance.

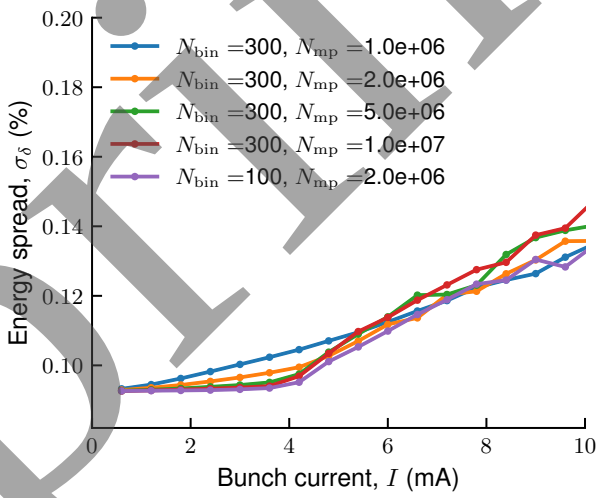

Figure 4: Convergence study for SOLEIL II impedance model excluding CSR contribution.

Simulation Parameters

All simulations are using parameters of SOLEIL II [2], different from the more computationally demanding case of SOLEIL (low momentum compaction mode), used in the previous section for benchmarking the implementation.

Figure 3 shows a convergence study on macroparticle and bin numbers for simulating CSR for SOLEIL II parameters. In this convergence study, only the CSR wake is included as a source of beam instability or bunch lengthening. All curves in Fig. 3 overlap indicating that for CSR already at $N_{\text{bin}} = 256$ bins and $N_{\text{mp}} = 1\,000\,000$ macroparticles the convergence is reached.

Figure 4 shows a convergence study on bin and macroparticle numbers for the impedance model of SOLEIL II, excluding CSR contribution. The displayed curves converge towards an instability threshold $\approx 4\,\text{mA}$. The threshold does not change with an increase in the number of bins, indicating that THz component of the impedance model does not drive MWI. Without the narrow peak in THz frequency region, the simulation parameters are determined by the require-

ments to resolve CSR impedance. This results in a relatively modest requirement on the number of macroparticles and bins. In that case, the instability thresholds are determined by lower frequency impedance. For the resistive-wall-driven MWI, the results are identical to the ones with impedance < 100 GHz [3]. The THz peak does not affect the threshold due to low NEG resistivity, in agreement with [9].

For all simulations, we are using our code `mbtrack2` [22, 23], including the following effects: radiation effects (damping and quantum excitation), intrabeam scattering, transverse one-turn map, chromaticity, and interactions with RF cavities, longitudinal short-range wakefields, and CSR wakefields. Sufficient sampling of wakefunction is chosen (0.1 ps) to resolve the THz frequency region. It was necessary to implement CSR wakefields in `mbtrack2` to have the combination of all relevant effects in the simulation.

Based on a convergence study, 10 000 000 macroparticles are tracked for 25 000 turns in all simulations; the bunches are sliced longitudinally into 512 bins for the wakefield and IBS interactions. The binning of the bunch for wake computations is done dynamically in `mbtrack2`, so the simulation starts with 512 bins to account for the eventual bunch lengthening (from zero-current 9 ps rms to $\approx$ 30 ps rms with all effects included, ($\approx$ 0.5 ps maximal bin width)).

SOLEIL II RESULTS

Figure 5 shows equilibrium rms energy spread, including the effects of CSR, IBS, and impedance. The shaded region

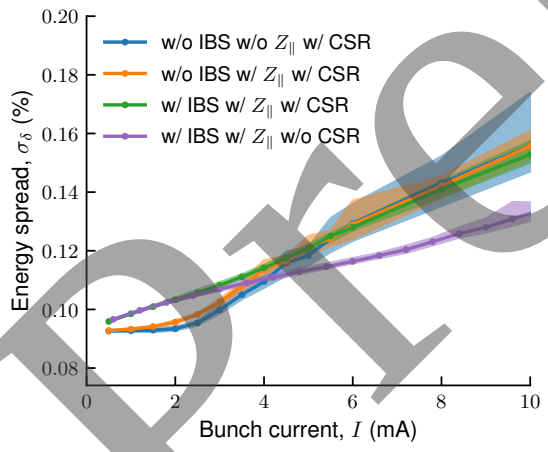

Figure 5: Energy spread (rms) as a function of bunch current.

of each curve shows the minimal and maximal energy spread during the bursting behaviour of MWI. Similar to [3], we consider the MWI threshold to be determined by the start of energy spread oscillations, as the mean value of energy spread will steadily grow with current due to IBS. The MWI threshold is $I_{\mathrm{th}} \approx 2$ mA without taking into account IBS, which is close to the analytical prediction of $I_{\mathrm{th}} = 1.6$ mA. CSR is shown to be the dominant contribution to the instability threshold. With all effects included, the energy spread increase at bunch currents $I_b \lesssim 3$ mA is dominated by IBS. Similar to [3], IBS also seems to decrease the bursting effect

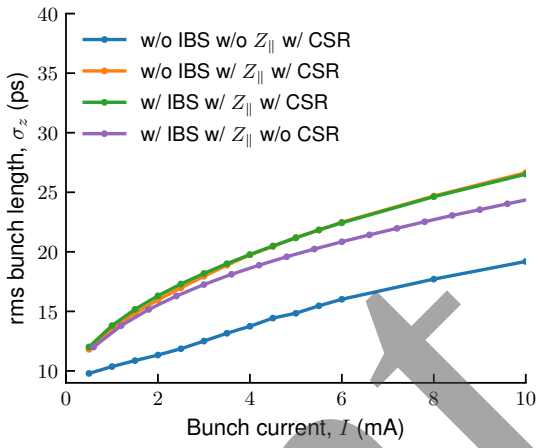

Figure 6: Bunch length (rms) as a function of bunch current.

after the instability threshold and to slightly increase the instability threshold itself. With CSR included, the equilibrium energy spread does not change for the 416-bunch operation mode but will slightly increase for 32-bunch mode.

Figure 6 shows the rms bunch length, including the effects of CSR, IBS and impedance. In the case of bunch length, the dominant contribution is from the impedance model, with CSR only increasing the bunch length a little bit further.

In our simulation study, we do not observe any effect of the THz peak of resistive wall impedance. This is attributed to a low NEG resistivity value expected for the SOLEIL II vacuum chamber, while the THz-driven microwave instability is expected for high-resistivity NEG [9] but can be mitigated if realistic NEG coating thickness distribution is considered [10].

CONCLUSION

CSR wakepotential was implemented in `mbtrack2` and benchmarked with previously published results and an analytical formula. The effect of CSR on microbunching instability threshold was investigated for the case of SOLEIL II storage ring. We find that in SOLEIL II the MWI threshold is dominated by the CSR contribution. CSR threshold is found to be above the 416 bunch mode nominal current (1.2 mA per bunch) without the effect of IBS. For 416-bunch mode, the energy spread is determined mostly by the IBS. For 32-bunch mode, the energy spread is determined by a combination of impedance, IBS and CSR. We find that inclusion of CSR in the simulation will slightly increase the bunch length and energy spread at bunch currents larger than 3 mA.

ACKNOWLEDGEMENTS

The authors are grateful to E. Roussel (University of Lille) for providing the original data (used in the benchmark) of [19] and for sharing the implementation details with us. Part of this work was performed using the CCRT HPC resource (TOPAZE supercomputer) hosted at Bruyéres-le-Châtel, France.

REFERENCES

[1] Synchrotron SOLEIL, "Conceptual Design Report - Synchrotron SOLEIL Upgrade", Synchrotron SOLEIL, White paper, Jul. 2021. https://www.synchrotron-soleil.fr/fr/file/13803/download?token=OUzsp46P

[2] A. Nadji and L. Nadolski, "Upgrade Project of the SOLEIL Accelerator Complex", *Synchrotron Radiat. News*, vol. 36, no. 1, pp. 10–15, Jan. 2023. doi:10.1080/08940886.2023.2186661

[3] V. Gubaidulin *et al.*, "Interaction of intrabeam scattering, longitudinal wakefield and a passive harmonic rf cavity in SOLEIL II", *J. Phys. Conf. Ser.*, vol. 3094, no. 1, p. 012030, Sep. 2025. doi:10.1088/1742-6596/3094/1/012030

[4] G. Stupakov and S. Heifets, "Beam instability and microbunching due to coherent synchrotron radiation", *Phys. Rev. Spec. Top. Accel. Beams*, vol. 5, no. 5, p. 054402, May 2002. doi:10.1103/PhysRevSTAB.5.054402

[5] K. L. F. Bane, Y. Cai, and G. Stupakov, "Threshold studies of the microwave instability in electron storage rings", *Phys. Rev. ST Accel. Beams*, vol. 13, no. 10, p. 104402, Oct. 2010. doi:10.1103/PhysRevSTAB.13.104402

[6] G. Stupakov and D. Zhou, "Analytical theory of coherent synchrotron radiation wakefield of short bunches shielded by conducting parallel plates", *Phys. Rev. Accel. Beams*, vol. 19, no. 4, p. 044402, Apr. 2016. doi:10.1103/PhysRevAccelBeams.19.044402

[7] S. Dastan *et al.*, "Coherent synchrotron radiation instability in low-emittance electron storage rings", *Phys. Rev. Accel. Beams*, vol. 27, no. 10, p. 104401, Oct. 2024. doi:10.1103/PhysRevAccelBeams.27.104401

[8] A. Gamelin and W. Foosang, "Influence of the coating resistivity on beam dynamics", *Phys. Rev. Accel. Beams*, vol. 26, no. 5, p. 054401, May 2023. doi:10.1103/PhysRevAccelBeams.26.054401

[9] W. Li, T. He, and Z. Bai, "Terahertz scale microbunching instability driven by high resistivity nonevaporable getter coating resistive-wall impedance", *Phys. Rev. Accel. Beams*, vol. 27, no. 3, p. 034401, Mar. 2024. doi:10.1103/PhysRevAccelBeams.27.034401

[10] D. Rabusov, I. PS. Martin, S. Wang, and R. T. Fielder, "Microwave instability driven by terahertz-scale resistive-wall impedance in electron synchrotrons", *Nucl. Instrum. Methods Phys. Res. A*, vol. 1072, p. 170147, Mar. 2025. doi:10.1016/j.nima.2024.170147

[11] V. Gubaidulin, A. Gamelin, A. Loulergue, R. Nagaoka, and P. Schreiber, "Transverse instabilities in SOLEIL II storage ring in the presence of a harmonic cavity", in *Proc. IPAC'24*, Nashville, TN, USA, May 2024. doi:10.18429/JACoW-IPAC2024-MOPS45

[12] A. Gamelin, V. Gubaidulin, R. Nagaoka, and S. Thakur, "Improved resistive wall effective radius taking into account yokoya factors", presented at IPAC'26, Deauville, France, May 2026, paper WEP5091, this conference.

[13] Y. Cai, "Linear theory of microwave instability in electron storage rings", *Phys. Rev. ST Accel. Beams*, vol. 14, no. 6, p. 061002, Jun. 2011. doi:10.1103/PhysRevSTAB.14.061002

[14] JB. Murphy, S. Krinsky, and RL. Gluckstern, "Longitudinal wakefield for an electron moving on a circular orbit", *Part. Accel.*, vol. 57, no. 1, pp. 9–64, 1997. https://cds.cern.ch/record/1120287/files/p9.pdf

[15] EL. Saldin, EA. Schneidmiller, and MV. Yurkov, "On the coherent radiation of an electron bunch moving in an arc of a circle", *Nucl. Instrum. Methods Phys. Res. A*, vol. 398, no. 2–3, pp. 373–394, Oct. 1997. doi:10.1016/S0168-9002(97)00822-X

[16] M. Borland, "Simple method for particle tracking with coherent synchrotron radiation", *Phys. Rev. Spec. Top. Accel. Beams*, vol. 4, no. 7, p. 070701, Jul. 2001. doi:10.1103/PhysRevSTAB.4.070701

[17] J. Qiang, C. Mitchell, and R. D. Ryne, "A fast high-order method to calculate wakefields in an electron beam", *Nucl. Instrum. Methods Phys. Res. A*, vol. 682, pp. 49–53, Aug. 2012. doi:10.1016/j.nima.2012.04.064

[18] C. E. Mitchell, J. Qiang, and R. D. Ryne, "A fast method for computing 1-D wakefields due to coherent synchrotron radiation", *Nucl. Instrum. Methods Phys. Res. A*, vol. 715, pp. 119–125, Jul. 2013. doi:10.1016/j.nima.2013.03.013

[19] E. Roussel, C. Evain, C. Szwaj, and S. Bielawski, "Microbunching instability in storage rings: Link between phase-space structure and terahertz coherent synchrotron radiation radio-frequency spectra", *Phys. Rev. Spec. Top. Accel. Beams*, vol. 17, no. 1, Jan. 2014. doi:10.1103/physrevstab.17.010701

[20] Eéonore. Roussel, "Spatio-temporal dynamics of relativistic electron bunches during the microbunching instability: study of the Synchrotron SOLEIL and UVSOR storage rings", Ph.D. thesis, Université Lille, Lille, France, 2015. https://theses.hal.science/tel-01112910v1

[21] A. Gamelin, "Collective effects in a transient microbunching regime and ion cloud mitigation in ThomX", Ph.D. thesis, Université Paris Saclay (COmUE), Sep. 2018. https://theses.hal.science/tel-01934906

[22] A. Gamelin, W. Foosang, and R. Nagaoka, "Mbtrack2, a Collective Effect Library in Python", in *Proc. IPAC'21*, Campinas, Brazil, May 2021. doi:10.18429/JACoW-IPAC2021-MOPAB070

[23] A. Gamelin, W. Foosang, N. Yamamoto, V. Gubaidulin, and R. Nagaoka, MBTRACK2, Synchrotron SOLEIL, Dec. 2024. doi:10.5281/zenodo.10871039